ADVANCED ELECTRONIC MATERIALS
www.advelectronicmat.de

A Biomimetic, Biocompatible OECT Sensor for the Real-Time Measurement of Concentration and Saturation of Ions in Plant Sap

Francesco Gentile, Filippo Vurro, Michela Janni, Riccardo Manfredi, Francesco Cellini, Angelo Petrozza, Andrea Zappettini, and Nicola Coppedè**

Currently, the transport of ions and nutrients in the plant stem is determined by destructive techniques or by radiolabeled compounds. Here, materials science and mathematical modeling have been combined to develop a sensor device that can monitor in real time and simultaneously the concentration of ions and the saturation in the plant's xylem. The device, based on the technology of organic electrochemical transistors, is biomimetic, biocompatible, low-cost, and minimally invasive. The mathematical model decodes the sensor's response and decouples the effects of concentration and saturation over time. In this work, this scheme is demonstrated by monitoring the condition of tomato plants subjected to vapor pressure deficit for 16 d, and to drought and salt stress for up to 25 d. Results of the work have the potential to impact on the analysis of plant's physiology, improve water use efficiency in small and large-scale agriculture, and maximize yield with a minimum amount of fertilizer/nutrients.

1. Introduction

Agriculture is at the basis of food and feed. Civilization itself is chiefly a history of agriculture. The Neolithic revolution, in which humans changed from being hunter-gatherers to a more permanent and settled lifestyle, was facilitated by a shift in agriculture.[1,2] The new practice of cultivating plants and domesticating crops granted access to a more reliable, more constant, and more sustainable source of food.[3] Today, agriculture produces the vast majority of the world's food supply.[1] Consequently, improving farming efficiency may accommodate the rapidly increasing global demand for food, reduce the world's water consumption, and mitigate the effects of climate change and global warming. Since farmers operate in a very time-sensitive environment with quickly shifting weather and environmental conditions, sensors for the real-time monitoring of a plant's condition should provide ways to manage better and more efficiently the parameters of farming, such as planned water delivery, the supply of nutrients or pesticides, and soil preparation. Moreover, since often fields and equipment are distributed over very large areas with sites also several kilometers distant, the farming industry can realize significant benefit from devices that allow remote sensing of plants, and that can be integrated in a network alongside with emerging Internet of Things (IoT) technologies.[4]

In this work, we demonstrate a biomimetic, biocompatible, and minimally invasive sensor device that can monitor in real time and simultaneously the concentration of ions and the saturation in the plant's xylem. The device combines the biomimetic structure of natural fibers with the sensing capability of conductive polymers to accomplish the continuous measure of the plant sap in a non-destructive fashion.[5] Data generated from the sensor are analyzed using a mathematical model to determine the concentration of ions in the sap and the values of saturation over time. The saturation is the fraction of plant's tissue permeated with the sap. While the sensor device and the algorithm have been independently demonstrated in previous studies,[5,6] their combination is new and does not have any precedent in the literature for the sensing technologies of plants.

The sensing organic electrochemical transistor (OECT) device is based on two textile functionalized electrodes introduced in the plant stem (**Figure 1**a,b).[5] One electrode is connected at both ends and is used as a transistor channel, the other electrode is the gate. The electrodes are bridged by the plant sap. Upon application of a positive potential at gate, cations of the system are forced into the polymeric channel and, as a result, the conductivity of the channel is reduced (Figure 1c). The biosensor (*bioristor*) measures the currents flowing from the gate (I_{gs}) and the drain (I_{ds}) (i.e., the ground) to the source electrode. Both I_{gs} and I_{ds} depend on the physical and chemical characteristics of

F. Gentile
Nanotechnology Research Center
Department of Experimental and Clinical Medicine
University of Magna Graecia
Catanzaro 88100, Italy
E-mail: francesco.gentile@unicz.it
F. Vurro, M. Janni, R. Manfredi, A. Zappettini, N. Coppedè
Institute of Materials for Electronics and Magnetism, IMEM-CNR
Parco Area delle Scienze 37/A, Parma 43124, Italy
E-mail: nicola.coppede@imem.cnr.it
F. Cellini, A. Petrozza
ALSIA Centro Ricerche Metapontum Agrobios
s.s. Jonica 106, km 448,2, Metaponto, MT 75010, Italy
The ORCID identification number(s) for the author(s) of this article can be found under https://doi.org/10.1002/aelm.202200092.

DOI: 10.1002/aelm.202200092

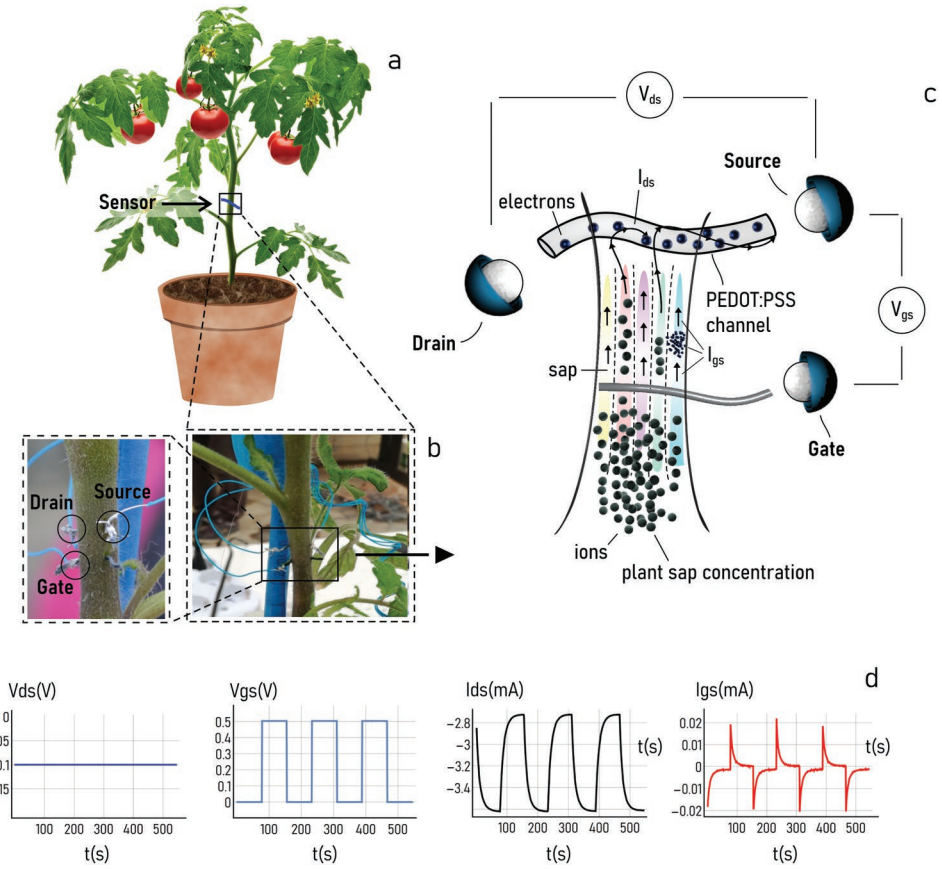

Figure 1. a) Illustration of a tomato plant with the device integrated into the plant stem. b) Detail of the stem showing the biosensor embedded in the plant and the wires connecting the sensor device to an external probe station for acquisition and analysis. c) Schematics of the sensor device: in the plant vasculature, upon application of an external voltage ions are driven towards the PEDOT:PSS channel, this generates a measurable current. d) Typical values of voltages applied at the drain (V_{ds}) and the gate (V_{gs}), and of currents measured from the device at the drain (I_{ds}) and the gate (I_{gs})—notice that the sensor device measures a continuous output until a constant value of voltage is applied to the system.

the system, on the concentration of ions in the plant sap (C), on to the portion of the body plant that is permeated with the sap (S)—expressed as a fraction of the system's volume (see the Experimental Section). As a consequence, a mathematical model that puts in relation the variables of the system can estimate C and S from the measured values of I_{gs} and I_{ds}.[6] Thus, while the *bioristor* performs an in vivo, continuous and accurate detection of the plant alterations encoded in an electric signal, the mathematical model decodes data and enables to derive information about the system under analysis.

Notably, this scheme enables quantification of the system without calibration of the device. In other words – the model has not internal variables that have to be tuned by experiment. For a fixed geometry and known physical/chemical characteristics of the device, the model provides a direct estimate of C and S without the need of preparatory test campaigns. However, while this is true in principle, a calibration procedure and comparison with a known reference is always preferable to avoid errors, especially when the characteristics of the electrodes and ions are uncertain. This aspect is discussed in detail later in the paper. Details on the mathematical model are reported in the Supporting Information S1.

Several platforms have been developed to study plant physiological process at subcellular, cellular, tissues, organ level up to the individual scale.[7] Nevertheless, many of these procedures are based on the morphological and morphometric screening of plants, such as the use plant imaging.[8] In contrast, biochemical analyses of plants are labor-intensive, time consuming, lower throughput, costly and frequently based on destructive methodologies.[9] Other studies have demonstrated sensors for the detection of heavy metal in plants,[10] for the detection of ions,[11] or for an estimate of the sap flow in the plants.[12] On the other hand, the existing models that decode the signal of OECT devices[13] are based on the approximation that the electrolyte is homogenous within the sample domain – with the consequence that the liquid content of the system is assumed constant, and variables such as the saturation are disregarded. None of the described approaches share the characteristics of low-cost, biocompatibility, real-time analysis of the system, nor allow the simultaneous and quantitative measure of the concentration of the intended species in the plant, and the evaluation of how much of the internal part of the plant is wet at a given time.

In contrast to other existing methods of plant analysis, in a recent work,[14] Strand and colleagues have developed state-of-the art printed organic electrochemical transistors for detecting nutrients in whole plant sap. The sensor device achieved high

current and voltage sensitivity, low limit of detection down to 0.01 *mM*, and was selective for the detection of potassium. However, while relevant in many aspects, this pioneering sensor device is not integrated in the plant's stem, it is not an in-vivo device, and the measurement itself is accomplished outside the plant. Thus, it does not perform a continuous measurement and necessitates of an external intervention to harvest the plant soup. For this, its use is not intended for long time data collection, differently from the *bioristor* that we have developed. Our device and methods thereof are of great significance and that can complement or improve the already important results obtained by Strand and collaborators.

The device presented in the work represents one of the first examples of integration of technological biomimetic solutions in biological living systems. Here, we demonstrate the method and its relevance in cases of interest in plant science, i.e., the analysis the tomato plants under vapor pressure deficit, drought and salt stress conditions.

2. Results

2.1. Plants Subject to Vapor Pressure Deficit Condition

We tested the device in tomato plants subjected to different types of abiotic stress as described in the Experimental Section. In a first experiment, we monitored in real time plants in an environment in which the vapor pressure deficit (VPD) was varied over time. The VPD describes the difference between the water vapor pressure at saturation and the actual water vapor pressure for a given temperature: it is an important driver of atmospheric water demand for plants.[15,16] The *bioristor* measured the gate-to-source (I_{gs}) and drain-to-source (I_{ds}) values of current resulting from this condition for more than 16 d. We then used data from the *bioristor* to determine the concentration of ions (**Figure 2**a) and the saturation in the plant's tissue (Figure 2b). We determined the best estimate of the values of concentration (C) and saturation (S) using a numerical procedure.

The algorithm determined C and S as those values that minimize a cost function ψ, expressed in terms of the characteristics of the system and of the values of I_{gs} and I_{ds} measured from the sensor device. The true values of C and S are such that $\psi \equiv 0$ (Experimental Section). The search for the solution was conducted in a finite variables-space where, due to physical limits of computation, ψ not always reached convergence to 0—in which case we estimated C and S as the values of the variables for which ψ settled to a minimum. Then, to improve accuracy, C and S were averaged over 10 local minima. Thus, the error bars in Figure 2a,b are relative to different numerical solutions associated to the same dataset. To assess the accuracy of the numerical procedure, we used an error metrics, i.e., the normalized difference between the minimum of ψ (measured value) and zero (expected value).

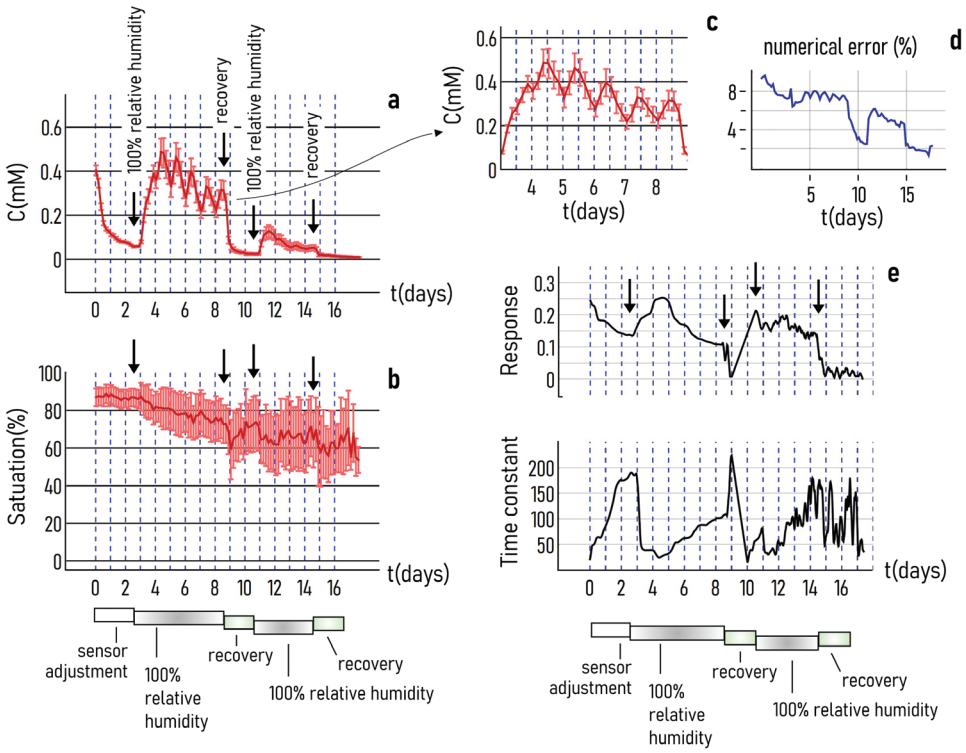

Figure 2. The values of a) concentration C and b) saturation S determined in a tomato plant subjected to a variable VPD condition for more than 16 d. c) Detail of day and night modulation of the sap ion concentration. d) The numerical error made by the algorithm in determining C and S. e) Response and time constant measured by the sensor device for the whole duration of the acquisition.

In analyzing the concentration profile (C) determined for plants subject to VPD we observe a cyclic variation of C over time (Figure 2a,c). The observed circadian variation in sap ion concentration (Figure 2c) is consistent with the existing literature reporting that higher concentration values occur during the night.[17] The basis for this difference has been suggested deriving from a greater rate of water extraction from the soil during the day, resulting in a higher degree of electrolyte dilution.[18] We report in a separate Supporting Information S2 further considerations and analysis pertaining the observed cyclic day-night alteration of the sensor response.

In the diagrams reported in Figure 2a,b, the origin of the time coordinate corresponds to the beginning of the acquisition process. We shall analyze the patterns of concentration first. After about 3 d from the beginning of the experiment, i.e., the settling time of the sensor, a 100% relative humidity (RH) condition is enforced in the system. As a result, the device measures a steep rise in the value of concentration of about a fourfold: from $C \approx 0.1 \times 10^{-3}$ M to more than $C \approx 0.4 \times 10^{-3}$ M, followed by a slow decrease of concentration: at day 8, $C \approx 0.25 \times 10^{-3}$ M. At day 8, the system is recovered to its initial state, i.e., the 100% RH condition is removed and the plant is exposed to standard relative humidity. Following these conditions, at day 9 the concentration falls to $C \approx 0.1 \times 10^{-3}$ M. At day 10, the 100% RH condition is again applied, causing a prompt rise and successive decrease of concentration. After removal of the 100% relative humidity condition at day 14, the value of concentration gradually drifts to zero, possibly caused by malfunctionings of the device.

The time pattern of concentration is consistent with the expected response of a plant to the described VPD variations. Upon application of the 100% RH—i.e., a rapid VPD decrease—the plant responds with a sudden reduction of plant transpiration and a strong reduction in the plant hydraulic conductance, and water flow in general.[19] This leads to a strong increase of ion concentration levels, until the VPD levels increase again and the transpiration stream is restored, with a relative reduction of the ion concentration in the xylem.

The observed response is consistent with the fact that every VPD increment influences plant transpiration due to stomatal closure.[16] Stomatal closure is a common adaptation response of plants to the onset of an external stress, such as drought, environmental or VPD variations.[16,20] Stomatal closure, in turn, reduces water loss.[21] Any VPD increment restores transpiration and thus water flow from roots to leaves—boosting in turn ion flux in the transpiration stream and reducing, as a result, ion concentration. The *bioristor* correctly measured such variations between day 4 and day 8. Notably, after restoring the system to its initial state at day 8, the descending trend of concentration is stopped.

Also notice that the repeated pattern of VPD (100% RH followed by plant recovery) between days 10 and 14 results in a pattern of concentration similar to that observed between days 2 and 10, but with a lower intensity, perhaps due to a loss of efficiency that the sensor device progressively experienced over time. Notably, this behavior is consistent with one of the first reported accounts of the effects of water movement on salt uptake in tomato plants.[22]

Figure 2b reports the saturation measured from the sensor throughout the 16 d of the experiment. While constant up to day 2, the saturation starts to decrease moderately immediately upon enforcing the 100% RH condition. Starting from an initial value of $S \approx 85\%$ of saturation, at the end of the measurement the system settles to $S \approx 60\%$, with an overall reduction of the 25%. This is consistent with the hypothesis of stomata closure under low VPD condition and the possible interruption of transpiration originating in the system over the 16 d of the experiment. This in turn may result in a reduction of the plant water loss, i.e., the water exchanged with the external of the plant, and consequently a decrease of the water uptake from the roots.[19,23] Notice also that, by decoupling the effects of concentration and saturation, we found that the variation of the sensor response is attributable more to variations of concentration, and less to variations of the saturation of the system.

Figure 2d illustrates the numerical error made in estimating the values of C and S throughout the experiment. Values of the error below the 8% indicate that the solution found by the model is accurate.

In Figure 2e, we report the response and the time constant measured from the sensor device. The response (R) is the difference between the I_{ds} measured from the sensor and a background value, relative to the background: $R = (I_{ds} - I_{ds}^{\circ})/I_{ds}^{\circ}$. The time constant ($\tau$) is the time necessary to the system to reach the 66% of its final value, it is measured in seconds. R and τ are variables commonly used to describe OECTs.[24] While sensitive to the stimuli applied to the system, the patterns of R and τ are less informative than the values of concentration and saturation derived through our model template. Moreover, it is not immediately clear how R and τ correlate. Being associated to physical observables of the system with an understandable significance, C and S provide a direct description of the system behavior. The algorithm that we have developed deconvolves the information encoded in the device's output and provide a more accessible insight of the physical behavior of the system.

2.2. Plants Subject to Drought Stress

We tested the performance of the method by examining a second case study, i.e., tomato plants subject to a drought cycle (Experimental Section). We used the I_{gs} and I_{ds} currents measured from the sensor to determine the values of concentration and saturation in the plant for over 25 d (**Figure 3**).

The pattern of stress was modulated as follows: *a*) from day 1 to day 5, the system is left at rest. *b*) At day 5, a drought stress is applied and maintained until day 19. *c*) At day 19, the system is brought to its initial state (recovery). *d*) At day 21, another condition of stress is applied.

Consequent to these stimuli, we observed that: i) upon application of the first stress condition the ion concentration in the plant continues to increase for 1 d, it oscillates around a mean value of $C \approx 0.5 \times 10^{-3}$ M until day 10, then it decreases steadily to $C \approx 0.4 \times 10^{-3}$ M at day 14. ii) Upon recovery to the initial condition, the system attains a maximum value of concentration $C \approx 0.6 \times 10^{-3}$ M at day 21 when iii), after the application of a second drought stress, the ion-concentration levels decrease and reach the value $C \approx 0.2 \times 10^{-3}$ M at day 25 (Figure 3a).

Notably, in the initial transient, the sensor device detects a value of concentration that steadily increases with time. In this

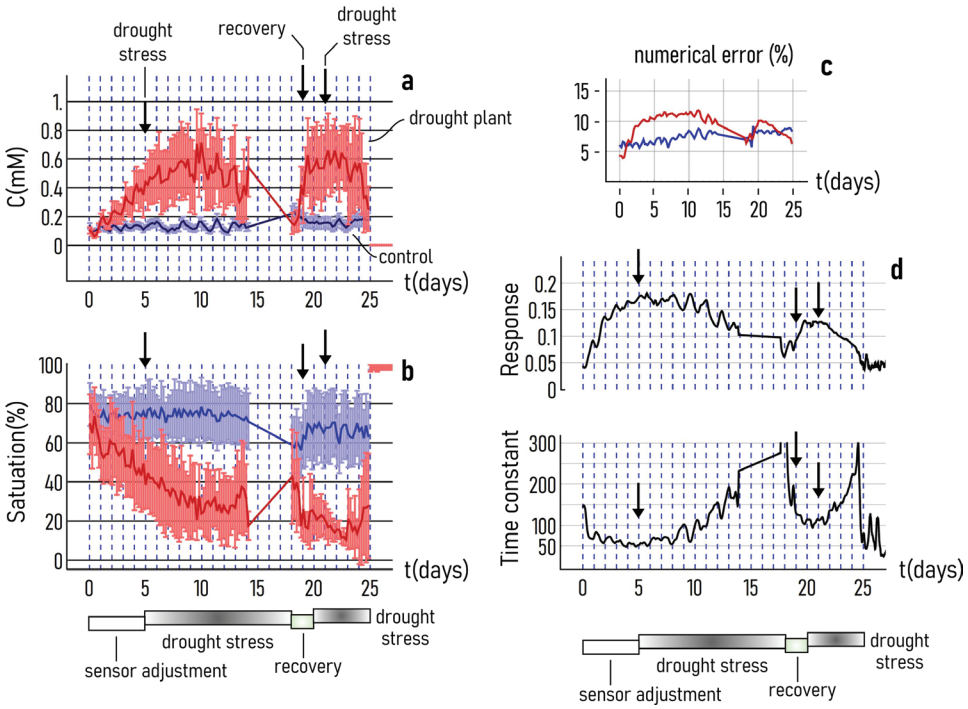

Figure 3. Values of a) concentration (*C*) and b) saturation (*S*) determined by the sensor device for a plant subjected to drought stress for 25 d, in red, compared to the values of *C* and *S* measured in the absence of drought stress, in blue. c) The numerical error made by the algorithm in determining *C* and *S*. d) Response and time constant of the system determined by the device.

phase, the response of the sensor tends to the hypothetical true value of concentration of ions in the plant, i.e., the adjustment phase. Notably, until day 2, there is a very high correspondence between the values of concentration measured in the stressed plant and the control. The differences between the stressed plant and the control following day 3, up to day 5, are explained considering that those are not-identical samples.

Differently from the values of concentration, the saturation in the plant transitions from an initial value of $S \approx 70\%$ at day 0 to $S \approx 30\%$ at day 25 (Figure 3b). Notably, from day 14 to day 18 there is a discontinuity in the acquisition window due to a malfunctioning of the device. The derived patterns of concentration and saturation—where to a condition of drought stress the system responds with a decrease of its ion concentration and a reduction of saturation—are consistent with the typical physiological reaction of a plant subjected to drought stress,[25] and with the direct measurements of C_a^{2+}, K^+ and N_a^+ ions in the plant sap performed in similar growing condition and upon the instauration of drought stress. The overall variation of ions content in the plant sap after 15 d in both regularly irrigated and drought stressed plants showed a strong decrease in the overall ion content (280 vs 188 $\times 10^{-3}$ M, respectively). This is in line with the observation that in response to severe drought stress plants close stomata to prevent water loss from transpiration pathways.[26]

The *bioristor* measures ions concentration and movements in the sieve tubes with a focus on xylem vessels since – as it is known – they provide an avenue for the unidirectional transport of water and mineral nutrients (xylem sap) from roots to aerial tissues that is driven by the transpiration stream.[27] A limited amount of mineral nutrients is transported in the phloem, thus *reasonably* the measurements performed with the LAQUAtwin system are representative of the overall plant sap circulating in the tomato sap and measured by the *bioristor*.

A reduction in water loss through stomatal closure and block of the transpiration stream, affect both concentration and saturation. The concentration decreases as a consequence of the compartmentalization of the ions to balance the water potential inside the plant xylem, on the other hand the water content in the plant decreases as effect of the block in transpiration and the reduced water uptake form the soil. The device correctly measured these changes. Results are especially relevant if compared to the control plants, i.e., tomato plant regularly irrigated with normal growth and physiological activity, for which the estimated values of concentration and saturation are nearly constant for the whole duration of the experiment. The numerical error made in estimating the values of the variables is limited between the 5% and the 11% for the considered time interval (Figure 3c). The values of R and τ reported for the system in Figure 3d illustrate again how these variables are less instructive of the condition of the system, compared to *C* and *S*.

2.3. Plants Subject to Salt Stress

We have examined the pattern of concentration and saturation in tomato plants subjected to salt stress to prove the core value of the technology that we have developed. After 2 d from the beginning of the measurements, tomato plants were watered with salt water with a concentration of 5 g L^{-1}, then increased

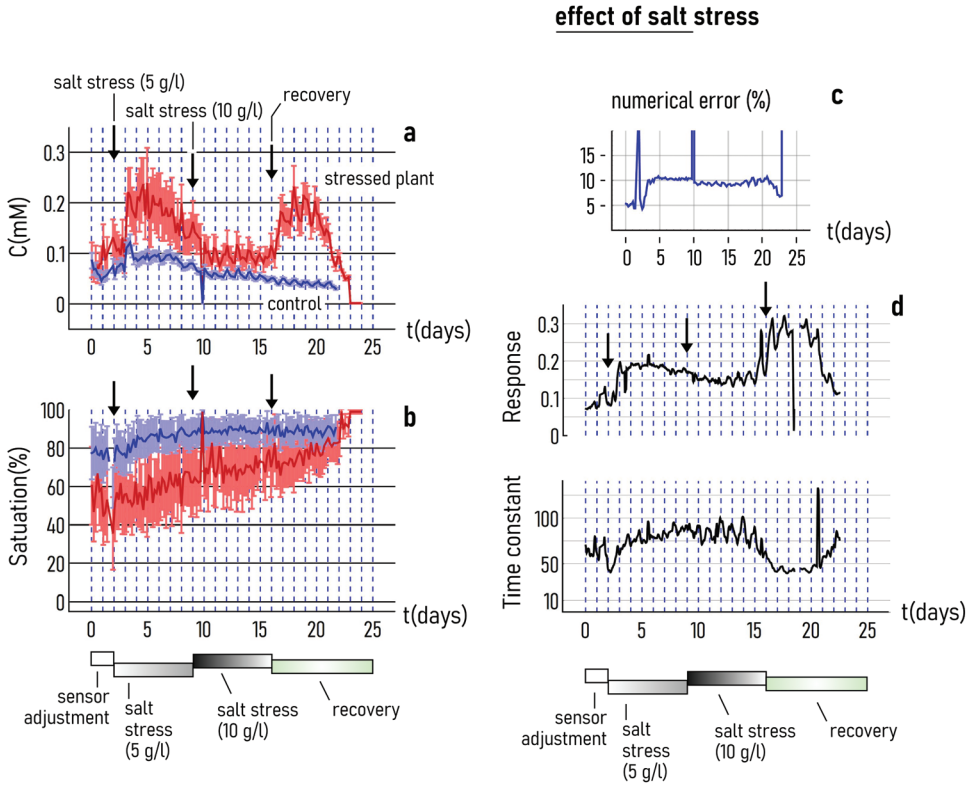

Figure 4. Values of a) concentration (*C*) and b) saturation (*S*) determined by the sensor device for a plant subjected to salt stress for 25 d, in red, compared to the values of *C* and *S* measured in the absence of salt stress (control), in blue. c) The numerical error made by the algorithm in determining *C* and *S*. d) Response and time constant of the system determined by the device.

to a value of 10 g L^{-1} at day 9 of the course of the experiment. After 16 d from time zero, tomato plants and the irrigation conditions were restored to normal prestress values (**Figure 4**a). Details on the experimental set-up and conditions are reported in the Experimental Section. The concentration of ions in the plant sap measured by our sensor device is consistent with the described salt-stress cycle. We observe that, every time that the plant is stimulated with a stress event, after an initial lag the system responds with a decrease in concentration. In effect, the concentration sharply increases from $C \approx 0.1 \times 10^{-3}$ M to more than $C \approx 0.2 \times 10^{-3}$ M between day 2 and 3—doubling its value in less than one day. Then, it is gradually brought to its initial value until day 16, when the recovery condition is applied. After which, the concentration rapidly fluctuates between a maximum ($C \approx 0.2 \times 10^{-3}$ M) and a minimum ($C \approx 0.05 \times 10^{-3}$ M), that is also the final value measured by the sensor device immediately before it is powered off.

The cyclic behavior of concentration and its variations are ascribable to the same mechanism invoked in the VPD and drought stress experiments. Upon application of the first stress, although in excess the salt in the water is adsorbed by the plant roots having, as an effect, an instantaneous rise of concentration in the vascular tissues. Then, the self-regulating mechanisms of the plant becomes active, leading to plant transpiration due to stomatal closure, that in turn reduces water loss and, consequently, the concentration of salts in the sap.[16,20] After recovery, plant stomata reopen, causing the immediate uptake of the residual salts left in the terrain and on the plant roots, followed by a stable reduction of concentration and the re-establishment of the initial state of the system.[28] Notably, in the considered period the saturation of the system smoothly transitions from an initial value of about $S \approx 50\%$ to a steady state value of $S \approx 80\%$ (Figure 4b). The continuous transformation of saturation, not directly nor proportionally related to the pattern of salt stress—differently from the concentration—indicates that the sensor device and the algorithm that we have developed are consistent. In the described case study, the error made in computing the solution oscillates between the 5% and the 10% for all the considered data points (Figure 4c). Moreover, the response and time constant variables associated to the experiment, reported in Figure 4d, are not obviously related to the salt stress applications—that again attributes to the concentration and saturation variables a particular value as indicators of the system and contributes to increase confidence in the results.

2.4. Biological Replicates of the Measurements and Statistical Analysis

To assess repeatability, reproducibility, and reliability we performed parallel measurements of biologically distinct samples. We analyzed 3, 4, and 4 different plants subject to VPD, drought stress, and salt stress respectively. The number of plants that we have used in this test campaign is not, by itself,

low, especially in acknowledgement of the fact that this study was not focused on optimizing performance. Moreover, each plant has been examined for up to 25 d, generating more than 1000 experimental data points per experiment, i.e., a vector with more than 1000 elements with the values of I_{gs}^{min}, I_{gs}^{max}, and I_{gs} measured by the sensor device over time. The values of concentration and saturation that we have extracted from the data were consistent within each experimental series, and across different datasets, as confirmed by the matching dissimilarity and correlation metrics as described below.

In Figure S3.1 (Supporting Information) we report the concentration and saturation profiles of plants subjected to a VPD condition, while Figure S3.2 (Supporting Information) illustrates the corresponding numerical errors. Figures S4.1 and S4.2 (Supporting Information) illustrate the response of plants to drought stress, with the errors shown in Figure S4.3 (Supporting Information). In the same way, in Figures S5.1–S5.3 (Supporting Information) we report additional salt stress experiments and the corresponding numerical errors.

Results indicate that, while not identical due to the intrinsic variability of biological systems, nonetheless the patterns of concentration and saturation in plants stimulated with VPD, drought and saline stress show similarities, proving the accuracy of the model and the reparability of the output of the sensor device. We performed a direct, quantitative comparison between the concentration profiles measured from the device for plants subjected to VPD (**Figure 5**), drought stress (**Figure 6**) and salt stress (**Figure 7**), to evaluate the extent to which results are consistent between different experiments.

2.5. Statistical Analysis of VPD Experiments

Figure 5a shows the concentration profiles in tomato plants bearing VPD variations measured in three different experiments. From process data signatures, for each experiment we determined special-cause variation events as those points in the pattern of concentration with a variation higher or equal than the 50% of the 2 d average. Then, we report results of the analysis in the raster plot of Figure 5b. In the plot, any significant or abnormal variation is represented as a black square (1) whereas white squares (0) indicate continuity in the data series. Thus, distributions of black and white points in the diagram, encoded mathematically in a sequence of 0 and 1, indicate the pattern of variation in the process caused by an external disturbance, i.e., the eternally applied VPD cycle. We then calculated the correlation and the matching dissimilarity between all the possible combinations of the Boolean vectors encoding the special cause variation in the time series, taken two at the time (Figure 5c). Values of correlation above zero (≈0.4), and of matching dissimilarity near zero (≈0.15)—statistically significantly different from the values of correlation (0) and dissimilarity (≈0.5) calculated between two random vectors of the same size—indicate that the VPD is the most likely origin of variation of the concentration in the plants (p-value = 0.05). Moreover, the low values of standard deviations associated to the correlation (sd = 0.11) and the matching dissimilarity (sd = 0.038) between the different pairs of vectors describing the concentration shifts, indicate low variability of the sensor's response to a VPD stimulus assessed through different experiments.

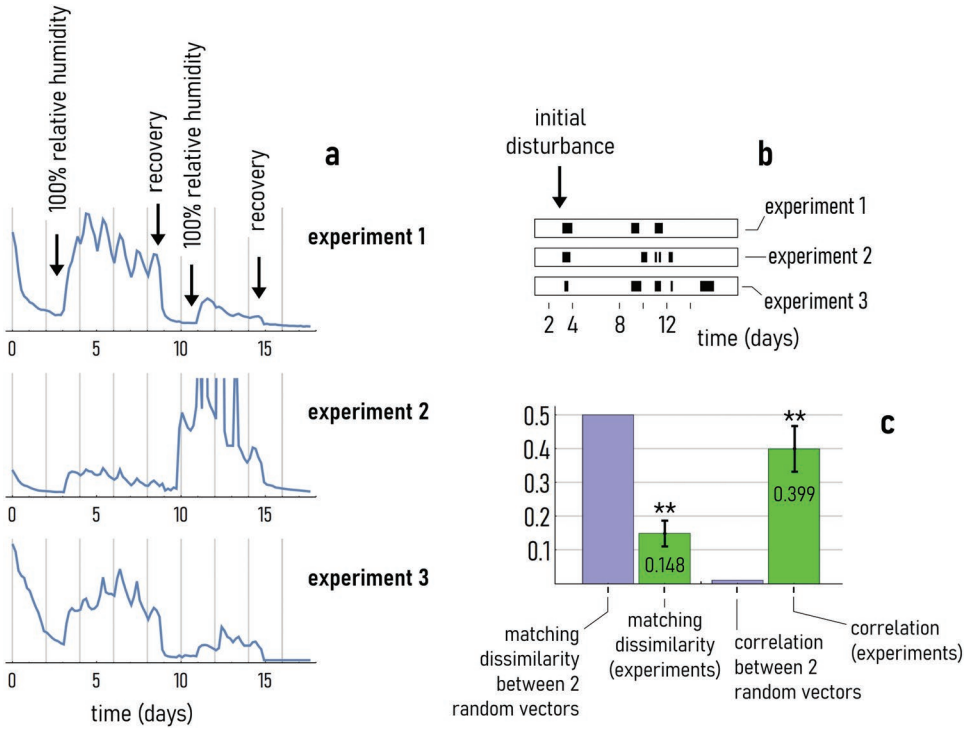

Figure 5. a) Concentration profile measured in plants subjected to the same VPD condition during three different experiments. b) Raster plots showing points of sudden change of concentration over time for the experiments reported in (a). c) The bar chart shows the value of matching dissimilarity and correlation measured between all the possible combinations of the patterns of significant variation reported in (b), compared to the values of matching dissimilarity (0.5) and correlation (0) describing random 0/1 vectors of the same size.

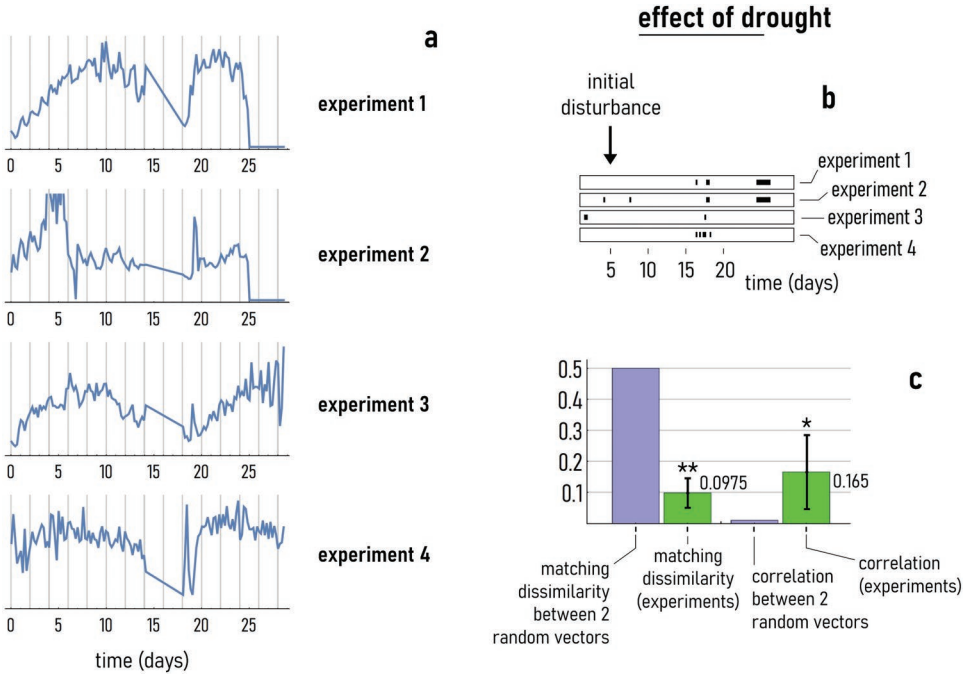

Figure 6. a) Concentration profile measured in plants subjected to the same drought stress during four different experiments. b) Raster plots showing points of sudden change of concentration over time for the experiments reported in (a). c) The bar chart shows the value of matching dissimilarity and correlation measured between all the possible combinations of the patterns of significant variation reported in (b), compared to the values of matching dissimilarity (0.5) and correlation (0) describing random 0/1 vectors of the same size.

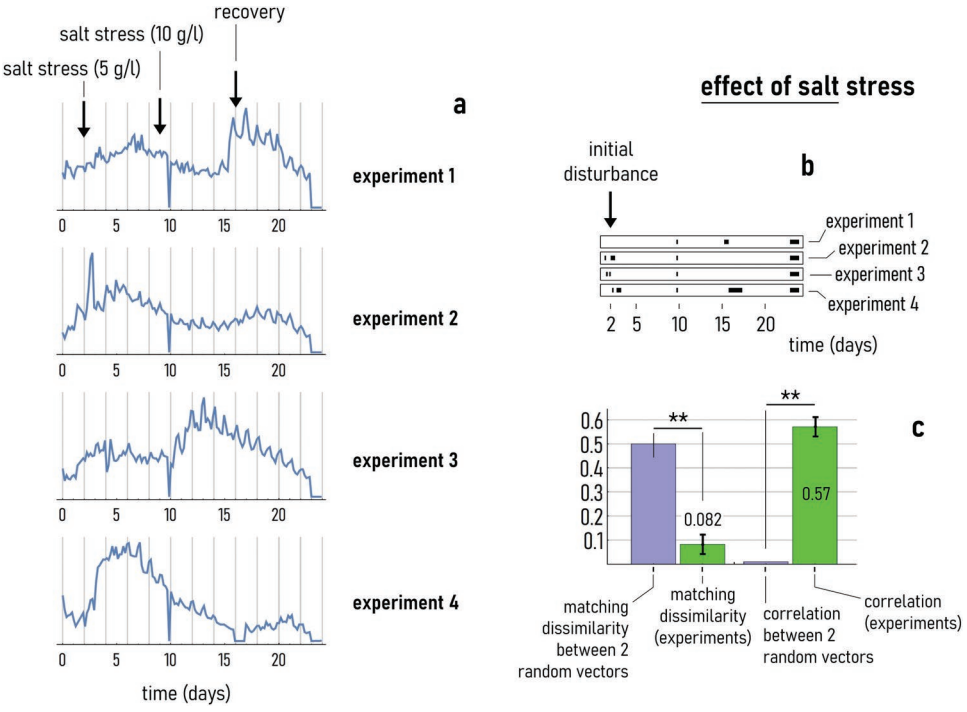

Figure 7. a) Concentration profile measured in plants subjected to the same salt stress cycle for four different experiments. b) Raster plots showing points of sudden change of concentration over time for the experiments reported in (a). c) The bar chart shows the value of matching dissimilarity and correlation measured between all the possible combinations of the patterns of significant variation reported in (b), compared to the values of matching dissimilarity (0.5) and correlation (0) describing random 0/1 vectors of the same size.

2.6. Statistical Analysis of Drought-Stress Experiments

We applied the same procedure to plants stressed with drought (Figure 6). We determined the patterns of concentration shift due to drought stress for four different experiments (Figure 6a,b). For this experimental set of measurements, we found the mean value of correlation and matching dissimilarity for all the possible combinations of the concentration-shift vectors as 0.165 and 0.0975, respectively. That, compared to 0 and 0.5 (that are the corresponding metrics applied to random data series of the same size) indicate repeatability of the sensor response. The correlation and matching dissimilarity values in the experiments, are statistically different from 0 with a p-value = 0.05, and from 0.5 with a p-value = 0.01. Moreover, for this set of measurements we calculated the standard deviations associated to the metrics of correlation and matching dissimilarity as 0.3 and 0.04, respectively.

2.7. Statistical Analysis of Salt-Stress Experiments

Analyzed on a statistical basis, the pattern of variations within the concentration profile for each of four of the biological repeats of the salt-stress experiments are internally and externally consistent (Figure 7a,b). For these experiments, the correlation and matching dissimilarity calculated between the different time series are ≈0.57 and ≈0.0.082, respectively (Figure 7c). These statistics measures are different from 0 and 0.5 (p-value < 0.01), which are the values that we would have found if the output of the sensor device were generated randomly (Figure 7c). Thus, for the diagrams of concentration in Figure 7 the salt stress is the most probable cause of variation. Moreover, the standard deviation relative to the correlation and dissimilarity calculated among different experiments is 0.04 and 0.39, respectively: low values of variance indicate very high repeatability of the sensor device.

3. Discussion and Conclusions

We have conceived a method based on an OECT biosensor and a mathematical model that can monitor in real time and non-destructively the plant activity up to several weeks. The method converts the output of the device, i.e., a current I, into values of concentration and saturation of the plant vascular tissues.

While the experimental campaign that we have performed in this study was aimed more at finding the patterns of variations of concentration and saturation, and less at determining their absolute values, it is however useful to put the values that we have determined in context. For the considered experiments, the values of concentration determined by the model fall in the $0–1 \times 10^{-3}$ M interval while, usually, the total concentration of ions in plant sap is in the $1–60 \times 10^{-3}$ M range. This discrepancy can be ascribed to the form of the resistivity $\rho(C)$ used in the model template, which reaches saturation for values of concentration higher than about 1×10^{-3} M. However, while the model underestimates the true physical values of concentration in the plant sap, performing an additional test campaign we have found a calibration formula that can be used to correct the model output and align the model results with the true values of concentration found in plants. Upon fitting of calibration data to a two-parametric linear function, we found that the concentration values can be adjusted using the equation $C_{\text{true}} = (C_{\text{model}} - a)/b$, with $a \approx 0.35 \times 10^{-3}$ M and $b \approx 0.035 \times 10^{-3}$ M. Thus, postprocessing of data returns values of concentration measured in the experiments correctly falling in the $1–185 \times 10^{-3}$ M interval: well within the range of concentration found in plants (Supporting Information S6). Remarkably, performing additional tests with an alternative method of analysis aimed to find an independent measure of the total concentration of ions in the plant sap—we found that the levels of concentration in the plant vascular tissues vary from $\approx 280 \times 10^{-3}$ to 190×10^{-3} M upon application of a drought stress (Supporting Information S7). In line with the qualitative and quantitative results of the *bior-istor* and the model template illustrated in this study.

Generally, the values of concentration and saturation are correlated to the physiological conditions of plants and to process such as transpiration rate, vapor pressure deficit, electrolytes composition in the ascending and descending sap streams, their conductance, water stress, temperature, pressure.[19,23,25] Optimal values of sap saturation and sap concentration of ions and metabolites would ensure their better nutrition, enhance plant performance, and reduce environmental impact. Hence, monitoring *in-vivo* sap saturation and concentration throughout the growing season is highly desirable to support environmentally friendly plant nutrition. This OECT biosensor and the mathematical model of data analysis will enable to decouple concentration and saturation, and to follow in real time the physiological changes in the plants. This may suggest innovative strategies to optimize nutrition and irrigation and consequently to reduce the environmental footprint of agriculture, at the same time allowing to identify the stages in which plant demand for nutrient is crucial for plant vegetative and reproduction activity.

Although the sensor device used in this study does not distinguish—in this current formulation—between different ions in the plant sap, some speculations can be done based on the physiological mechanisms triggered in the plant response following abiotic stresses. One of the major players in stress signaling is calcium: its abundance can be likely detected by the sensor device. Calcium plays a key role in processes that preserve the structural and functional integrity of plant membranes, stabilize cell wall structures, regulate ion transport and selectivity, and control ion-exchange behavior as well as cell wall enzyme activities. It is well known that the C_a^{2+} apoplastic flux is significantly dependent on the transpiration rate,[29] however, when C_a^{2+} is distributed in the vacuoles, then it's hardly redistributed to the remaining organs and parts of the plant. Water flow is also regulated by C_a^{2+} via its effects on the cell wall and stomatal aperture while apoplastic transportation leading to hypothesise that in the drought stress events a rapid increase of the sensor response is caused by the dislocation over long-distances of calcium, its accumulation and storage in the cell-vacuole, and by a consequent decrease of motility of C_a^{2+} in the sap.

The rate of C_a^{2+} transported in the plant is however strongly dependent on the overall cation balance. The exchange and internal trafficking of ions such as K^+, M_g^{2+}, N_a^+, NH^{4+} , and H^+ reduce the uptake of C_a^{2+} ions and their distribution in the plant tissues: that is interpreted by the sensor device as reduction of

the values of concentration (Figure 3a). During salt stress, a rapid rise in cytosolic C_a^{2+} levels has been reported within seconds from exposure to salt stress. This abundance of C_a^{2+} is, in turn, strongly influenced by the Na^+ uptake and can significantly increase during the stress as correctly evidenced by the increase of concentration illustrated in Figure 4a.[30] Moreover, results of the model support the hypothesis that an High VPD in a greenhouse contributes significantly to photosynthetic limitation, yield loss, and calcium deficiency.[19,31] Thus, the overall results achieved by the *bioristor* highlight its ability in increasing the knowledge relative to calcium-mediated response to abiotic stress.

Moreover, results obtained with the *bioristor* supports the physiological interpretation of the plant response to water and saline stress, as well as to changes of the environmental conditions.

It is well established that the stomatal closure is the simplest defense of a plant to limited water availability as it allows to minimize the loss by transpiration. Plant turgor and leaf water potential are conventionally used as indicators of water status.[28,32] Results of the model template evidence the role of the *bioristor* in detecting alterations (negative variations) of the transpiration leaves, resulting in stomatal closure and, indirectly, in the compartmentalization of ions during the stress. These mechanisms and the relationship between the response of the *bioristor* and the plant behavior, provides way to investigate short- and long-term signaling that occurs during abiotic stress in plants.

The sensor device that we have developed has nonetheless some weaknesses that need to be discussed. It does not distinguish between different ions in the plant sap. Moreover, the mathematical model that decodes the data from the sensor has as internal parameters the *resistivity* associated to one sole analyte. Thus, the *bioristor* is not selective and the concentration measured by the device and determined through the algorithm is an average of the concentrations of all the species that at a given instant of time are dissolved in solution. Likewise, the value of resistivity used in the model can be the combination of several different electric resistivities, the identification of which can be laborious or inaccurate. To improve resolution, accuracy, and selectivity, in a more sophisticated evolution that will be developed over time the sensor device will be equipped with ion exchange membranes. These membranes, integrated on the electrodes, will contribute to convert the activity of *specific* ions dissolved in the system into an electric potential. At the same time, the model will be improved to incorporate multiple ions, a non-linear multi parameter fit or artificial intelligence algorithms will separate variables in the sensor response—identifying them correctly.

4. Experimental Section

The OECT Sensor-Device: The sensor device used in this study is an OECT, *bioristor*, with the channel, and the drain, source, and gate electrodes directly integrated into the plant (Figure 1a,b). The biocompatibility of the device was demonstrated in other published reports.[5,33,34] The device was fabricated, installed, and operated following the methods reported in ref. [34] for the VPD experiments, and ref. [33] for the drought stress experiments. The channel of the OECT was inserted through the stem of the plant, then it was connected at both ends to a metal wire to form the *source* and the *drain* electrodes (Figure 1b,c). The connections were secured through silver paste. Then, a *gate* electrode completed the design of the sensor device (Figure 1b,c). The device was then connected to a controlled by a NI USB-6343 multifunction I/O device (National Instruments, Austin, TX, USA). A fixed constant voltage (V_{ds} (t) = $V_{ds,o}$) was applied between the drain and the source across the channel of the OECT. At the same time, an alternate stepwise voltage was implemented at the gate (V_{gs} = sign($V_{gs,o}2\pi/T\,t$)) (Figure 1d), where t is time, T = 200 s is the period of the voltage applied at the gate, "sign" is the sign function, $V_{ds,o}$ = − 0.1 V, and $V_{gs,o}$ = 0.8 V. Upon application of the voltages at the gate, and between the drain and the source, the currents I_{ds} (flowing in the channel) and I_{gs} (flowing in the plant) were generated in the system. I_{ds} and I_{gs} were monitored continuously for the entire duration of the experiments. The form of the I_{ds} current recalls the output of a first-order-system, transitioning from an initial (I_o) to a steady state value (I_f).[24,34] I_o is the current measured by the device when V_{gs} = 0, and R (the response of the system) is obtained as $R = (I_f - I_o)/I_o$.

Measuring the Electric Activity of the Plants Using the OECT: The operating principle of an OECT is thoroughly described in ref. [24]. Salts in the plant sap (NaCl, KCl, MgCl, ZnCl, and other salts) dissociate as cations (M^+) and anions (A^-). Upon application of a positive voltage at the gate, anions react at the gate electrode through a redox process, while cations are forced towards the PEDOT:PSS channel. The PEDOT:PSS channel is the same channel that in the previous section "The OECT Sensor-Device" was termed as OECT channel. The channel is the active part of the OECT device and is made of the conducting polymer PEDOT:PSS. The redox process of anions at the gate has in turn two effects. i) The redox process at the gate generates a Faradaic current (I_{gs}) flowing in the source-gate circuit [35] (Figure 1c). ii) At the same time, in contact with the channel cations de-dope the PEDOT:PSS polymer. De-doping results in the removal of the charge carriers from the conducting polymer. The smaller number of holes available for conduction in the channel is a consequence of the incorporation of cations in the PEDOT:PSS as described by Equation (1)

$$PEDOT^+:PSS^- + M^+ + e^- = PEDOT + M^+:PSS^- \quad (1)$$

cations adsorbed into the $PEDOT^+:PSS^-$ cause a reduction of the oxidized $PEDOT^+$ and inducing a decrease in conductivity upon reduction to PEDOT. This is a de-doping process because cations incorporated in the channel cause a reduction of the current of *electrons* flowing from the drain to the source (I_{ds}) (Figure 1c). Thus, the sensor device measures a current of *electrons* flowing in the channel from the drain to the source, which is proportional to the current of *cations* that run from the plant to the channel. For this, sometimes OCETs are called ions-electron transducers. Remarkably, the entire process is reversible: when the voltage between the gate and the source non-active (V_{gs} = 0), ion diffusion from the channel to the electrolyte increases the number of conducting holes and, consequently, I_{ds}.[13] In this configuration, the gate and the drain are the cathodes, and the source is the anode, thus positive charges move in the plant from the gate to the source, and in the channel from the drain to the source.

Measuring Plant Activity under a Controlled VPD Condition: The experiment to evaluate the ability of the sensor to monitor the physiological changes on the plant induced by the environmental variation of VPD was conducted according to ref. [34]. Three tomato plants of the cultivar Ikram were grown in 2.6 L pots until the initial stage of flowering development in a 0.4 m^3 growth chamber with a photoperiod of 16 h and relative humidity (RH) values between 55% and 70%. Thanks to the equipment of the growth chamber with an EasyLog data-logger (Lascar Electronics Ltd., Salisbury, UK), the temperature (T) and RH have been monitored to calculate the VPD value as described in ref. [34]. Upon reaching the last vegetative phase of the plants, a bioristor was inserted into the stem of each plant between the third and fourth leaves. All plants were well irrigated over 2 d postinsertion and were exposed to a decrease of the initial VPD (1 kPa) reaching values close to 0 within 24 h and keeping them until day 8, when VPD was rapidly increased (0–7 kPa). From 10 to 14 d, the VPD was again altered to confirm the previously observed mechanisms.

Measuring Plant Activity under a Controlled Drought Stress: The drought stress experiment was set up to demonstrate the ability of the *bioristor* to detect the physiological changes that occur in plants when they are deprived of water. The cultivar Red Setter seeds used were provided by ALSIA Metapontum Agrobios Research Center. Four tomato plants of the cultivar Red Setter were grown up to the stage of fifth fully expanded leaves in 1.5 dm^3 soil-filled pots under controlled conditions as described in ref. [33] (T = 24 °C, RH = 50%, photoperiod = 16 h). The plants were kept fully irrigated until their fifth true leaf had fully expanded, after which a *bioristor* was inserted in the stem of each plant. After three days, the irrigation of 44 plants was suspended for 12 d, the plants were then irrigated over 2 d (recovery), before being subjected to a second water stress of 6 d to validate the result obtained in the first one. Drought-stress results were validated using an independent method of analysis. In this case, the sap was extracted from three stems and the K^+, C_a^{2+}, and N_a^+ concentration determined on a handheld Horiba LAQUAtwin K^+ meter, LAQUAtwin C_a^{2+} meter and LAQUAtwin N_a^+ meter (HMIK, Kyoto, Japan). The output of the ions concentration in ppm has been converted in mM. A mean of the measured ions was reported as representative of the overall concentration of ions in the plant sap.

Measuring Plant Activity under a Controlled Saline Stress: The saline stress was set up to demonstrate the ability of bioristor to detect in vivo the onset of the defense mechanism that the plant put in place under salt stress. Plants of the tomato cultivar Ikram were grown in ALSIA Metapontum Agrobios Research Center. Eight plants were grown up to the stage of fifth fully expanded leaves in 1.5 dm^3 soil-filled pots under controlled conditions as described for the drought stress. Then, four plants after 2 d from the beginning of the experiment were irrigated with a 5 g L^{-1} NaCl solution while four plants were regularly irrigated and kept as controls. The salt stress was increased after 6 d increasing the NaCl concentration to 10 g L^{-1}. Reaching 16 d of treatment, plants were recovered through conventional irrigation.

Control Experiments: The VPD and drought experiments were carried on simultaneously. For the whole duration of the experiments, tomato plants were monitored under the same external and environmental conditions of the other tests, and used as a control. The control has been reported only once in the drought experiments diagrams.

The Model Template and Data Analysis: The OECT sensor device that was fabricated, measures for each applied value of voltage, the current transients at the gate (I_{gs}) and the drain (I_{ds}) from an initial to a final state. Each of these currents is a function of the type $I = \text{const}(1 - \exp(-t/\tau))$, where t is time, τ is the time constant of the system, and const is a constant. When voltages externally applied to the system are turned off, the current falls to a background value. The model that was developed in this study describes a transient of current in terms of the sole initial (I_{ds}^{min}, I_{gs}^{min}) and final (I_{ds}^{max}, I_{gs}^{max}) values of the variables measured by the OECT at each cycle. Thus, while the device monitors continuously the condition of a plant over time, the response of the system is discretized into a finite number of intervals. Each interval has a duration T, i.e., the number of seconds over which a constant voltage is applied. For each interval, measured values of I_{ds}^{min}, I_{ds}^{max} and I_{gs}^{max} were used to estimate the values of concentration (C) and saturation (S) within the system. To find C and S we solved the following set of equations [6] at each interval:

$$I_{ds}^{max} - I_{gs} = \frac{V_{ds}}{R_{ds}^{dry} + \left(\frac{R_o}{\text{mod}(C)+1} AS - R_{ds}^{dry} S\right)} \tag{2}$$

$$I_{ds}^{min} = \frac{V_{ds}}{R_{ds}^{dry} + \left(R_o AS - R_{ds}^{dry} S\right)} \tag{3}$$

$$I_{gs} = V_{gs} \frac{\phi}{\rho(C) l} AS \tag{4}$$

The derivation procedure of the equations can be found in ref. [6] and are reported for convenience in the Supporting Information S1. In the equations, V_{ds} and V_{gs} are the values of voltages applied at the drain and the gate. mod(C) is the modulation of the PEDOT:PSS channel, i.e., the increased value of current measured in the system resulting from a non-zero value of concentration C, mod (C) = $(I(C) - I_0)/I_0$. mod(C) is determined experimentally. I_0 is a reference value of current. It is the current flowing through the PEDOT:PSS channel from the drain to the source measured when the potential at the gate is not active, V_{gs} = 0. Thus $I_0 = I_{ds}$ (V_{gs} = 0). It indicates the state of rest of the system: it is akin to a baseline for the system. For any value of V_{gs} different from zero, ions in the plant sap are transported into the PEDOT:PSS channel, de-dope it, causing variation in the device response that is proportional to the concentration of ions in the system and to the saturation. R_{ds}^{dry} is the electrical resistance of the dry PEDOT channel before being exposed to the electrolyte. R_o is the resistance of the wet PEDOT channel after being exposed to the electrolyte. φ and l are the cross-sectional area diameter and length of an ideal small path connecting the part of the plant connected to the gate to that connected to the drain.

The internal resistance function $\rho(C)$ is a measure of the opposition to the Faradaic current flow (I_{gs}) in the plant body in the parts comprised between the gate and the channel. Consider the plant body ideally divided into slices, or circuits, as those painted in different colors in Figure 1. Each of these slices may either be or not be wet with the plant sap. The fraction of slices wet with the plant is S, the *saturation*. Thus S = 1 indicates a plant completely drenched with sap, conversely S = 0 indicates a dry plant body. The slices that are not wet with the plant sap, offer an infinity resistance to the transport of charges. Instead, slices that are wet with the plant sap enable the passage of charges with a resistance that is proportionate to the *concentration* of ions in that slice

$$\rho(C) = 0.0123 + \left(3647.5/C^{0.955}\right) \tag{5}$$

where the concentration is expressed in ppm and ρ is measured in $\Omega\ m^{-1}$.[6] The formula that was used to relate the concentration of ions to the resistance of the circuit is strictly valid for sodium chloride (NaCl).[36] Nevertheless, in this study, a simplifying assumption was made that all the salts dispersed in the system behave, to a first approximation, as sodium chloride with respect to their electrical properties. This approximation enabled to derive the governing equations of the model and the profiles of concentration and saturation in the systems. Thus, the concentration of the originating ions enters into the model through the electrical resistivity of the solution and Equation (5). Notice though that in the equation the symbol C represents the concentration of the salts in solution. It is not the ionic strength. In the specific case where a 1:1 electrolyte (sodium chloride) was considered, where each ion was singly charged, the ionic strength was equal to the concentration—but this was not the rule. There is possibly a method to generalize the model to other salts in solution. This would necessitate to reformulate Equation (5) and write the resistance ρ as a function of the concentration of all ions present in a solution. This can possibly be done using the molar ionic strength: $Is = \sum_n c_i z_i^2/2$, where Is is calculated taking into account the charges z and concentrations c of all the ions in the system. Then, the resistance or conductivity of the solution should be expressed in terms of Is, as it has be done, as for example, for sea water by Malmberg already in 1964.[37] Moreover, $I_{gs} = I_{gs}^{max}$ and A = 100. Further to this end, the values of electrical resistivity of the saline solution depend, as it is known, on the value of temperature to which the system is subjected. All the experiments of the study have been conducted at a temperature varying between 18 °C during the night and 24 °C during the day. For simplicity, in the model a value of resistivity of the ion-sap solution determined for a working temperature of 21 °C was used, i.e., the mathematical average between 18 and 22 °C.

Numerical Solutions to Equations: Since variables in Equations (2)–(4) were linked in a nonalgebraic way, a numerical procedure was used to find a root of the governing equations of the OECT device. The equations that describe the systems were of the form $\xi = \Upsilon(C, S)$. The ξ's were values of current measured by the device: they were known terms. The

Υ's were a function of the variables of the system including the unknown values of concentration (C) and saturation (S). With these premises, if $\psi = \xi - \Upsilon(C, S)$ is set, then the values of C and S such that $\psi = 0$ represent a solution of the system of equations. Finding the optimal values of concentration and saturation that satisfy the equation is therefore equivalent to minimize the absolute value of ψ. The nearest the value of ψ is to 0 the closer the estimates of C and S to the true values. For each experiment, the optimal values of the variables were searched in a domain where the saturation and the concentration were varied between 0 and 1 (S), and 0.1 and 10 times an initial guess of C. In case the algorithm failed to converge in the prescribed domain, an alternative search domain was used with iterated reweighted lower and upper boundaries for C. In the search for the roots of the equations, the values of C and S were accepted as solutions of the system if the difference between prediction of the model (Υ) and the output of the device (ξ) stays below 10%, i.e., if $e = (\xi - \Upsilon)/\xi < 0.1$. The code used to compute C and S is reported in a public data repository accessible through the link reported in the *Data Availability Statement* section for convenience of the reader interested to elaborate on the model even further. Notice though that this test campaign was not focused on optimizing algorithm performance and was more aimed to demonstrate that a biocompatible sensor device combined to a mathematical model can detect over time the conditions of a living system accurately and nondestructively.

Statistical analysis: Data in the diagrams are represented as mean ± standard deviation. A comparison between different vectors of 0 and 1 describing the amount of variation in the concentration profiles using two different metrics were performed, i.e., the correlation function (*corr*) and the matching dissimilarity function (*md*). Mathematically, the correlation function of two vectors v_1 and v_2 is $corr\ (v_1,v_2) = cov(v_1,v_2)/(sd(v_1)\ sd(v_2))$, where *cov* is the covariance and *sd* stands for standard deviation. The function correlation gives the Pearson's correlation coefficient between v_1 and v_2, i.e., is a statistic that measures linear correlation between variables. The matching dissimilarity function of v_1 and v_2 is equivalent to $(n_{10} + n_{01})/\text{length}(v_1)$, where n_{ij} is the number of corresponding pairs of elements in v_1 and v_2 respectively equal to i and j. Pairwise comparisons between means of different groups were performed using a Student's t-test (two tailed, unpaired) where, for each couple of normally distributed populations, the null hypothesis that the means are equal was verified. Everywhere in the text the difference between two subsets of data is considered statistically significant if the Student's t-test gives a significant level P (P value) less or equal than 0.05.

Supporting Information

Supporting Information is available from the Wiley Online Library or from the author.

Acknowledgements

The project was partially supported by Italian ministry of Agriculture RGV FAO (DM 10271), the E-CROPs project (PON—Programma Operativo Nazionale Ricerca e Innovazione 2014–2020 -ARS01_01136). The authors thanks ALSIA (Agenzia Lucana di Sviluppo e di Innovazione in Agricoltura) for the financial support of F.V. during his Ph.D. and for the ongoing scientific collaboration.

Open Access Funding provided by Universita degli Studi Magna Graecia di Catanzaro within the CRUI-CARE Agreement.

Conflict of Interest

The authors declare no conflict of interest.

Author Contributions

F.G. developed the mathematical model, analyzed data, and wrote the manuscript. F.V. performed the experiments on the plants and helped to write the manuscript. M.J. supervised the biological part of the work and put results in a biological context. R.M. produced and characterized the sensor devices. F.C. and A.P. contributed to perform the salt stress experiments. A.Z. contributed to develop the bioristor and supervised the experimental part of the work. N.C. designed and fabricated the bioristor, conceived the idea, designed the experimental plan, and helped in writing the manuscript. All authors discussed data, commented on the results, and revised the manuscript.

Data Availability Statement

The data that support the findings of this study are available from the corresponding author upon reasonable request.

Keywords

biological systems, mathematical modeling, organic electrochemical transistors, plant analysis, sensor devices

Received: January 24, 2022
Revised: May 2, 2022
Published online: June 12, 2022

[1] Johns Hopkins home page, http://www.foodsystemprimer.org/food-production/history-of-agriculture (accessed: January 2022).
[2] a) R. W. Bulliet, P. K. Crossley, D. R. Headrick, L. L. Johnson, S. W. Hirsch, *The Earth and Its Peoples: A Global History*, Vol. *I*, Houghton Mifflin, Boston, MA **2008**; b) D. D. Montgomery, *The Erosion of Civilizations*, University of California Press, Berkeley and Los Angeles, California **2008**; c) S. J. Parikh, B. R. James, *Nat. Educ. Knowl.* **2012**, *3*, 2.
[3] J. M. Diamond, *Guns, Germs, and Steel: The Fates of Human Societies*, W. W. Norton & Company, New York **1999**.
[4] a) O. Elijah, T. A. Rahman, I. Orikumhi, C. Y. Leow, M. N. Hindia, *IEEE Internet of Things J.* **2018**, *5*, 3758; b) S. C. Mukhopadhyay, N. K. Suryadevara, in *Internet of Things. Smart Sensors, Measurement and Instrumentation*, Vol. *9* (Ed: S. Mukhopadhyay), Springer, Cham, **2014**; c) A. Tzounis, N. Katsoulas, T. Bartzanas, C. Kittas, *Biosyst. Eng.* **2017**, *164*, 31.
[5] N. Coppedè, M. Janni, M. Bettelli, C. L. Maida, F. Gentile, M. Villani, R. Ruotolo, S. Iannotta, N. Marmiroli, M. Marmiroli, A. Zappettini, *Sci. Rep.* **2017**, *7*, 16195.
[6] F. Gentile, F. Vurro, F. Picelli, M. Bettelli, A. Zappettini, N. Coppedè, *Sens. Actuators, A* **2020**, *304*, 111894.
[7] R. Pieruschka, H. Poorter, *Funct. Plant Biol.* **2012**, *39*, 813.
[8] N. Fahlgren, M. A. Gehan, I. Baxter, *Curr. Opin. Plant Biol.* **2015**, *24*, 93.
[9] a) T. R. I. Cataldi, G. Margiotta, A. Del Fiore, S. A. Bufo, *Phytochem. Anal.* **2003**, *14*, 176; b) J. E. Delmore, A. D. Appelhans, *Biol. Mass Spectrom.* **1991**, *20*, 237; c) P. B. Gahan, A. K. Rajan, *J. Exp. Bot.* **1966**, *17*, 34.
[10] a) O. Krystofova, L. Trnkova, V. Adam, J. Zehnalek, J. Hubalek, P. Babula, R. Kizek, *Sensors* **2010**, *10*, 5308; b) M. A. Palacios, Z. Wang, V. A. Montes, G. V. Zyryanov, P. Anzenbacher, *J. Am. Chem. Soc.* **2008**, *130*, 10307.
[11] P. Romele, P. Gkoupidenis, D. A. Koutsouras, K. Lieberth, Z. M. Kovács-Vajna, P. W. M. Blom, F. Torricelli, *Nat. Commun.* **2020**, *11*, 3743.
[12] a) T. W. Davis, C.-M. Kuo, X. Liang, P.-S. Yu, *Sensors* **2012**, *12*, 954; b) S. A. James, M. J. Clearwater, F. C. Meinzer, G. Goldstein, *Tree Physiol.* **2002**, *22*, 277.
[13] D. A. Bernards, G. G. Malliaras, *Adv. Funct. Mater.* **2007**, *17*, 3538.

[14] E. J. Strand, E. Bihar, S. M. Gleason, S. Han, S. W. Schreiber, M. N. Renny, G. G. Malliaras, R. R. McLeod, G. L. Whiting, *Adv. Electron. Mater.* **2021**, *8*, 2100853.
[15] H. M. Rawson, J. E. Begg, R. G. Woodward, *Planta* **1977**, *134*, 5.
[16] W. Yuan, Y. Zheng, S. Piao, P. Ciais, D. Lombardozzi, Y. Wang, Y. Ryu, G. Chen, W. Dong, Z. Hu, A. K. Jain, C. Jiang, E. Kat, S. Li, S. Lienert, S. Liu, J. E. M. S. Nabel, Z. Qin, T. Quine, S. Sitch, W. K. Smith, F. Wang, C. Wu, Z. Xiao, S. Yang, *Sci. Adv.* **2019**, *5*, eaax1396.
[17] K. Mengel, E. Kirkby, *Principles of Plant Nutrition*, Kluwer Academic Publishers, Dordrecht **2001**.
[18] G. Tarabella, M. Villani, D. Calestani, R. Mosca, S. Iannotta, A. Zappettini, N. Coppedè, *J. Mater. Chem.* **2012**, *22*, 23830.
[19] D. Zhang, Q. Du, Z. Zhang, X. Jiao, X. Song, J. Li, *Sci. Rep.* **2017**, *7*, 43461.
[20] S. Agurla, S. Gahir, S. Munemasa, Y. Murata, A. S. Raghavendra, in *Survival Strategies in Extreme Cold and Desiccation*, Vol. *1081* (Eds: M. Iwaya-Inoue, M. Sakurai, M. Uemura), Springer, Singapore **2018**.
[21] L. T. Bertolino, R. S. Caine, J. E. Gray, *Front. Plant Sci.* **2019**, *10*, 225.
[22] W. Lopushinsky, *Plant Physiol.* **1964**, *39*, 494.
[23] a) M. J. Devi, V. R. Reddy, *Front. Plant Sci.* **2018**, *9*, 1572; b) E. Merilo, D. Yarmolinsky, P. Jalakas, H. Parik, I. Tulva, B. Rasulov, K. Kilk, H. Kollist, *Plant Physiol.* **2018**, *176*, 851.
[24] N. Coppedè, M. Villani, F. Gentile, *Sci. Rep.* **2014**, *4*, 4297.
[25] a) A. Bahrun, C. R. Jensen, F. Asch, V. O. Mogensen, *J. Exp. Bot.* **2002**, *53*, 251; b) Y. Hu, Z. Burucs, S. von Tucher, U. Schmidhalter, *Environ. Exp. Bot.* **2007**, *60*, 268; c) E. C. Silva, R. M. Nogueira, M. A. Silva, M. B. Albuquerque, *Plant Stress* **2011**, *5*, 32.
[26] H. Pirasteh-Anosheh, A. Saed-Moucheshi, H. Pakniyat, M. Pessarakli, in *Water Stress and Crop Plants: A Sustainable Approach*, Vol. *1* (Ed: P. Ahmad), John Wiley & Sons, Ltd, Oxford (UK) **2016**, p. 24.
[27] P. Carella, D.-C. Wilson, C.-J. Kempthorne, R.-K. Cameron, *Front. Plant Sci.* **2016**, *7*, 651.
[28] M. Janni, C. Cocozza, F. Brilli, S. Pignattelli, F. Vurro, N. Coppede, M. Bettelli, D. Calestani, F. Loreto, A. Zappettini, *Sci. Rep.* **2021**, *11*, 18598.
[29] M. Gilliham, M. Dayod, B.-J. Hocking, B. Xu, S.-J. Conn, B.-N. Kaiser, R.-A. Leigh, S.-D. Tyerman, *J. Exp. Bot.* **2011**, *62*, 2233.
[30] X. Yu, M. Zhao, X. Wang, X. Jiao, X. Song, J. Li, *Environ. Exp. Bot.* **2022**, *195*, 104786.
[31] P. Kupper, G. Rohula, L. Inno, I. Ostonen, A. Sellin, A. Sober, *Reg. Environ. Change* **2017**, *17*, 2149.
[32] D. Danzi, N. Briglia, A. Petrozza, S. Summerer, G. Povero, A. Stivaletta, F. Cellini, D. Pignone, D. De Paola, M. Janni, *Front. Plant Sci.* **2019**, *15*, 15.
[33] M. Janni, N. Coppede, M. Bettelli, N. Briglia, A. Petrozza, S. Summerer, F. Vurro, D. Danzi, F. Cellini, N. Marmiroli, D. Pignone, *Plant Phenomics* **2019**, *6*, 168209.
[34] F. Vurro, M. Janni, N. Coppedè, F. Gentile, R. Manfredi, M. Bettelli, A. Zappettini, *Sensors* **2019**, *19*, 4667.
[35] G. Tarabella, C. Santato, S. Yoon Yang, S. Iannotta, G. G. Malliaras, F. Cicoira, *Appl. Phys. Lett.* **2010**, *97*, 123304.
[36] a) P. C. Ho, D. A. Palmer, R. E. Mesmer, *J. Solution Chem.* **1994**, *23*, 997; b) T. Isono, *J. Chem. Eng. Data* **1984**, *29*, 45.
[37] C. G. Malmberg, *J. Res. Natl. Bur. Stand., A* **1964**, *69A*, 39.